

FUELCELL2006-97271

EXPERIMENTAL INVESTIGATION OF LIQUID WATER FORMATION AND TRANSPORT IN A TRANSPARENT SINGLE-SERPENTINE PEM FUEL CELL

Dusan Spornjak

Suresh Advani

Ajay K. Prasad

Fuel Cell Research Laboratory
Department of Mechanical Engineering, University of Delaware, Newark, DE 19716

ABSTRACT

Liquid water formation and transport was investigated by direct experimental visualization in an operational transparent single-serpentine PEM fuel cell. We examined the effectiveness of various gas diffusion layer (GDL) materials in removing water away from the cathode and through the flow field over a range of operating conditions. Complete polarization curves as well as time evolution studies after step changes in current draw were obtained with simultaneous liquid water visualization within the transparent cell. At similar current density (i.e. water production rate), lower level of cathode flow field flooding indicated that liquid water had been trapped inside the GDL pores and catalyst layer, resulting in lower output voltage.

No liquid water was observed in the anode flow field unless cathode GDLs had a microporous layer (MPL). MPL on the cathode side creates a pressure barrier for water produced at the catalyst layer. Water is pushed across the membrane to the anode side, resulting in anode flow field flooding close to the H_2 exit.

INTRODUCTION

Humidification has to be carefully optimized in polymer electrolyte membrane fuel cells (PEMFC). Extremes in humidity levels at both the low end (membrane dehydration) and the high end (cathode flooding) of the range can significantly reduce PEMFC performance. Due to these conflicting requirements, the window for operating conditions for a PEMFC is very narrow. The cell is usually operated at the flooding limit, and some areas of the catalyst layer can be covered by condensing water. Since flooding has been identified as one of the main current-limiting processes, understanding and optimizing liquid water transport throughout the cell is critical to improving PEMFC performance. Moreover, flooding can also take place at lower current densities, if the gas flow rate and/or temperature (i.e. equilibrium vapor pressure) are low [1-6].

Various experimental techniques have been employed to investigate water dynamics in PEMFC. Membrane dehydration is commonly observed through the increase in the cell (i.e. membrane) resistance [1, 7]. To detect cathode flooding, one

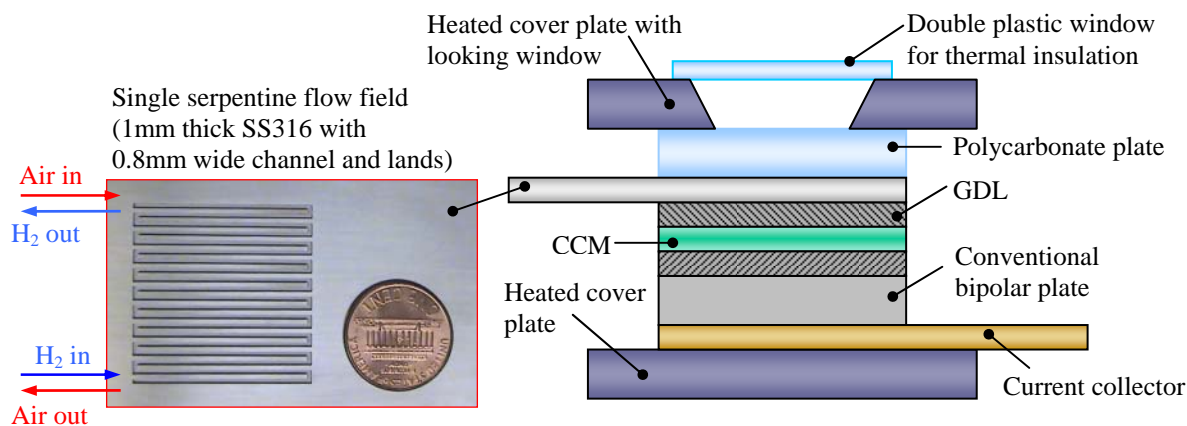


Fig. 1. Operational transparent PEMFC

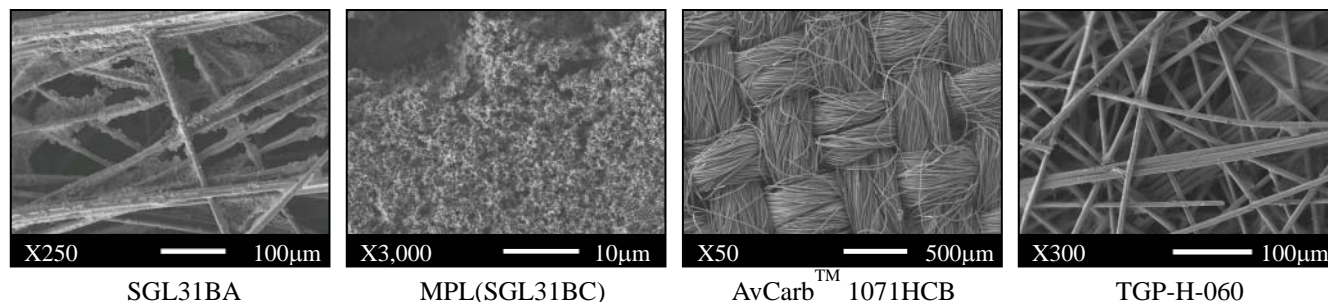


Fig. 2. SEM images of GDL microstructure

can use *global* tools such as fully saturated air at the exit [1] and increase in the pressure drop [2,6]. Flooding is also associated with a drop in the cell output power. *Local* information about the flooded regions in the cell can be obtained by current and temperature distribution measurements [5]. When water is still in the vapor phase, higher temperature regions correspond to higher current. Condensed water leads to lower current density in flooded areas, accompanied by local increase in temperature due to the release of latent heat of condensation. Besides aforementioned physical indicators of flooding (current, temperature, pressure drop, and relative humidity), various *imaging techniques* can be employed to investigate two-phase dynamics inside the cell. Known possibilities are direct flow visualization [5,6,8,9], neutron radiography [10], and magnetic resonance imaging [11].

Although direct flow visualization requires a special cell design (Fig. 1), it is a very attractive experimental technique since optical access to the channels provides high spatial and/or temporal resolution, depending on the combination of optics and recording equipment. Moreover, modeling efforts focusing on two-phase flow through the porous GDL, e.g. [3,4], suggest that experimental data are needed to validate and improve the

models. Most of the published work with transparent hydrogen-air cells investigates parallel flow field configurations, and has been limited to the cathode side. The objective of our present research is to examine the two-phase flow inside a single-serpentine PEMFC by direct experimental visualization. We address the influence of different gas diffusion layers (GDLs) on water management, as well as the effect of the microporous layer (MPL). Two series of visualization experiments were performed, in which cathode and anode sides were visualized.

Experimental

To compare the water management effectiveness of GDL materials, several membrane-electrode assemblies (MEAs) were fabricated with the same catalyst coated membrane (CCM) while varying the GDL. The CCM used was a 25 µm thick Nafion®-based membrane with 0.3 mg/cm² Pt loading on each side (Ion Power, Inc.). The GDL materials tested are listed below (Fig. 2):

- Sigracet® SGL31BA by SGL Carbon Group
- Sigracet® SGL31BC and SGL35BC (both with MPL) by SGL Carbon Group
- AvCarb™ 1071HCB by Ballard®
- TGP-H-060 by Toray Industries, Inc.

MEAs were first tested in a conventional 10 cm² PEMFC (by Fuel Cell Technologies), with a single serpentine channel cut into Poco Durabraz® graphite bipolar plates. The channel was 0.8 mm wide and 1 mm deep, with 0.8 mm wide lands. A 200 W test station, from Arbin Instruments, was used for monitoring and control of flow, pressure, temperature, humidity and electronic load. Humidity of the gas was controlled by the dew point temperature (DPT) in the humidifier. All tests were done at 1 bar backpressure, with constant flow rates (expressed in standard liters per minute). For conversion to stoichiometries, 0.18 slpm of air and 0.076 slpm of hydrogen correspond to 1 A/cm² equivalent flow rate for our 10 cm² cell.

Formation and transport of liquid water was observed using an operational, transparent PEMFC (Fig. 1). The transparent cell has a single serpentine channel cut through a 1 mm thick stainless steel plate, which also serves as the current collector (Fig. 1). Visual access is allowed through a polycarbonate cover plate. The other half of the cell was retained from the aforementioned conventional cell, with the

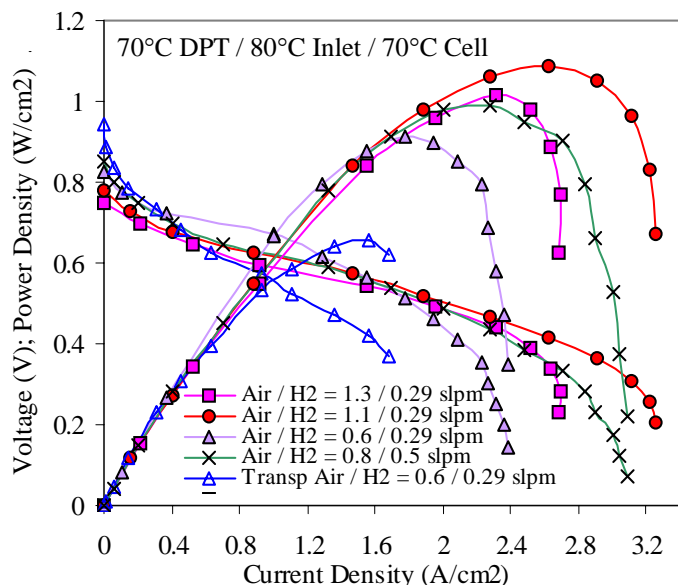


Fig. 3. Influence of flow rates with SGL31BA as GDL

graphite bipolar plate. Our approach has been to stay as close to the real life situation as possible: standard stainless steel 316 was used for the flow field, and fogging of the polycarbonate plate was mitigated by heating the cell. In contrast, the anti-fog coating employed in [8], which is a surfactant in nature, could modify the surface properties of the channel wall, thus influencing the two-phase transport through the channel.

A digital camcorder (Sony DCR-HC42) was used for imaging (1 frame per minute). Since our goal was to obtain a global estimation of the flow field flooding, magnification was set to show about 60% of the flow field, which is acceptable since no liquid water was commonly observed in the upstream portion. Flow direction in all cell tests and the corresponding

images of the cathode and anode side is as indicated in Fig. 1. Portions of some images are shown enlarged, to better visualize liquid water formation and transport.

Influence of Operating Conditions

Figure 3 shows the effect of flow rates in the conventional cell, with SGL31BA as the GDL. At high flow rates and/or high operating temperature, membrane dehydration is observed through lower performance curves, as well as increased current oscillations at constant voltage, and confirmed later in the transparent cell. An additional curve from the experimental transparent cell is shown for comparison. As expected, the transparent cell performance was lower than the conventional

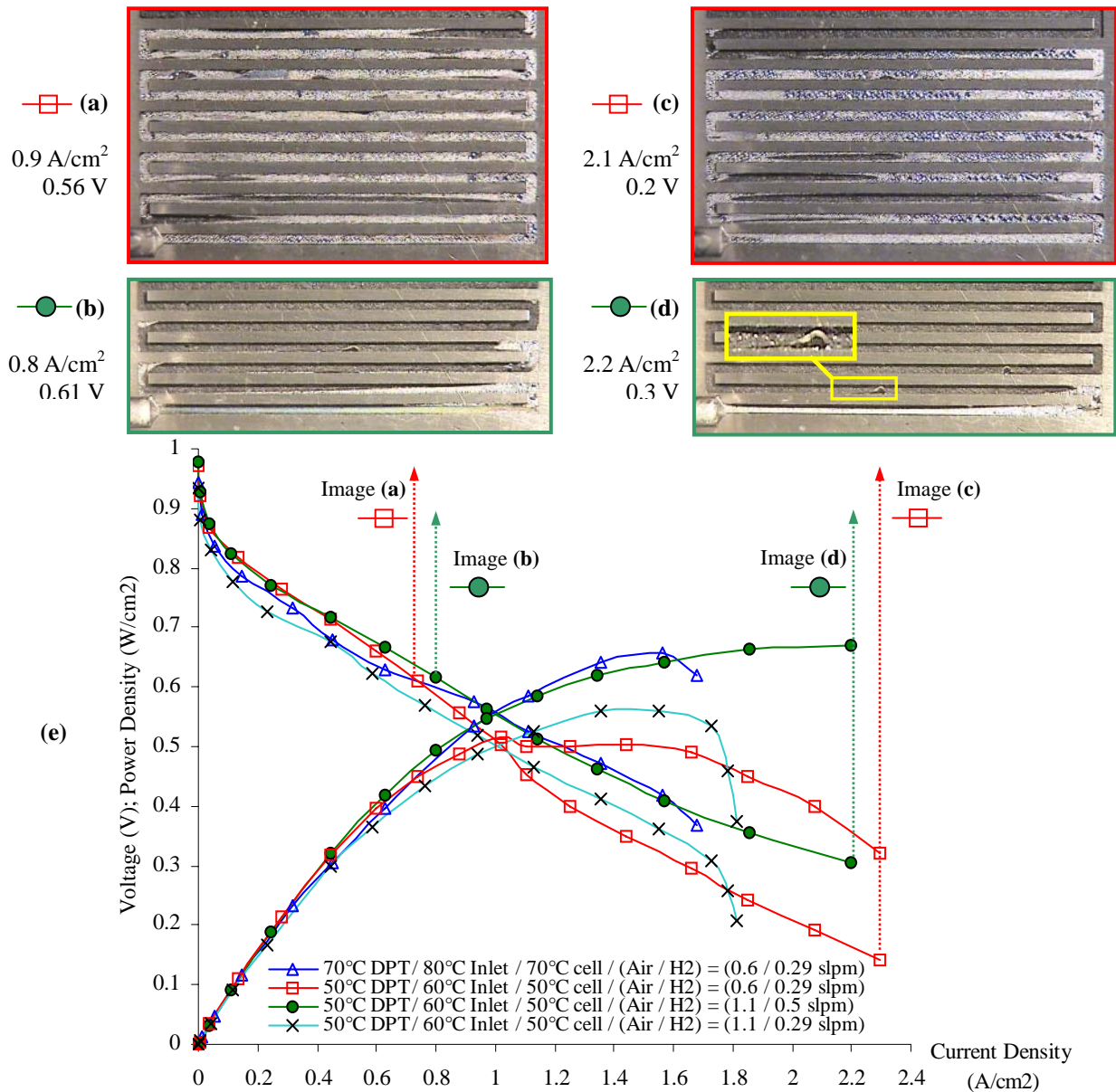


Fig. 4. (a)–(b), (c)–(d): Cathode flow field flooding compared at similar current density while recording the polarization curves (e) Performance curves of the transparent cell with SGL31BA at different operating conditions

cell, mostly due to lower current collecting and conducting ability of the thin steel plate. Next, the influence of operating parameters was investigated in the transparent cell, with SGL31BA as the GDL (Figs. 4, 5). After condensing in the vicinity of the catalyst layer of the cathode side, liquid water is wicked away from the porous electrode through the GDL capillaries into the channels. Droplets emerge at preferential locations on the GDL surface and keep growing until swept by the gas stream and other coalescing droplets. When the growing droplets come in contact with the (more hydrophilic) channel walls, they either spread into a thin film, or, if the gas flow rate is too small, they continue to grow, occupying a large portion of the channel cross section. In addition, liquid water in the flow field arises from condensation on the top channel wall (usually more pronounced at U-turns), as a consequence of the imperfect temperature controls of the experimental cell. A similar situation can be expected in an industrial fuel cell stack, which is often cooled by circulating coolant through channels in the bipolar plates.

Images in Fig. 4 depict the influence of flow rates on the

cathode flow field flooding, compared at two current densities for the cell at 50°C. At similar current density (i.e. similar water production rate), the amount of liquid water in the cathode channels is much higher at low flow rates (especially for low air flow rate). Although the performance is very similar at lower current densities for the images shown, the difference in the two-phase transport is substantial (compare the images (a) and (b) in Fig. 4.). Next, at 50°C and high air flow rate of 1.1 slpm, slightly better performance with higher H₂ flow rate suggests that membrane hydration was helped by the anode gas flow. This is also supported by the fact that there was no visible water when the H₂ flow rate was low.

Further, cell response at constant voltage 0.4 V (Fig. 5) was recorded after switching from open circuit (OCV). After initial flooding due to the sudden jump in current draw, the cell operating at higher flow rates (Fig. 5b) managed to recover and reach a steady state. At lower flow rates (Fig. 5a), the cell continued to operate with a partially flooded cathode flow field. At higher operating temperature (70°C, Figs. 4e, 5c), almost no

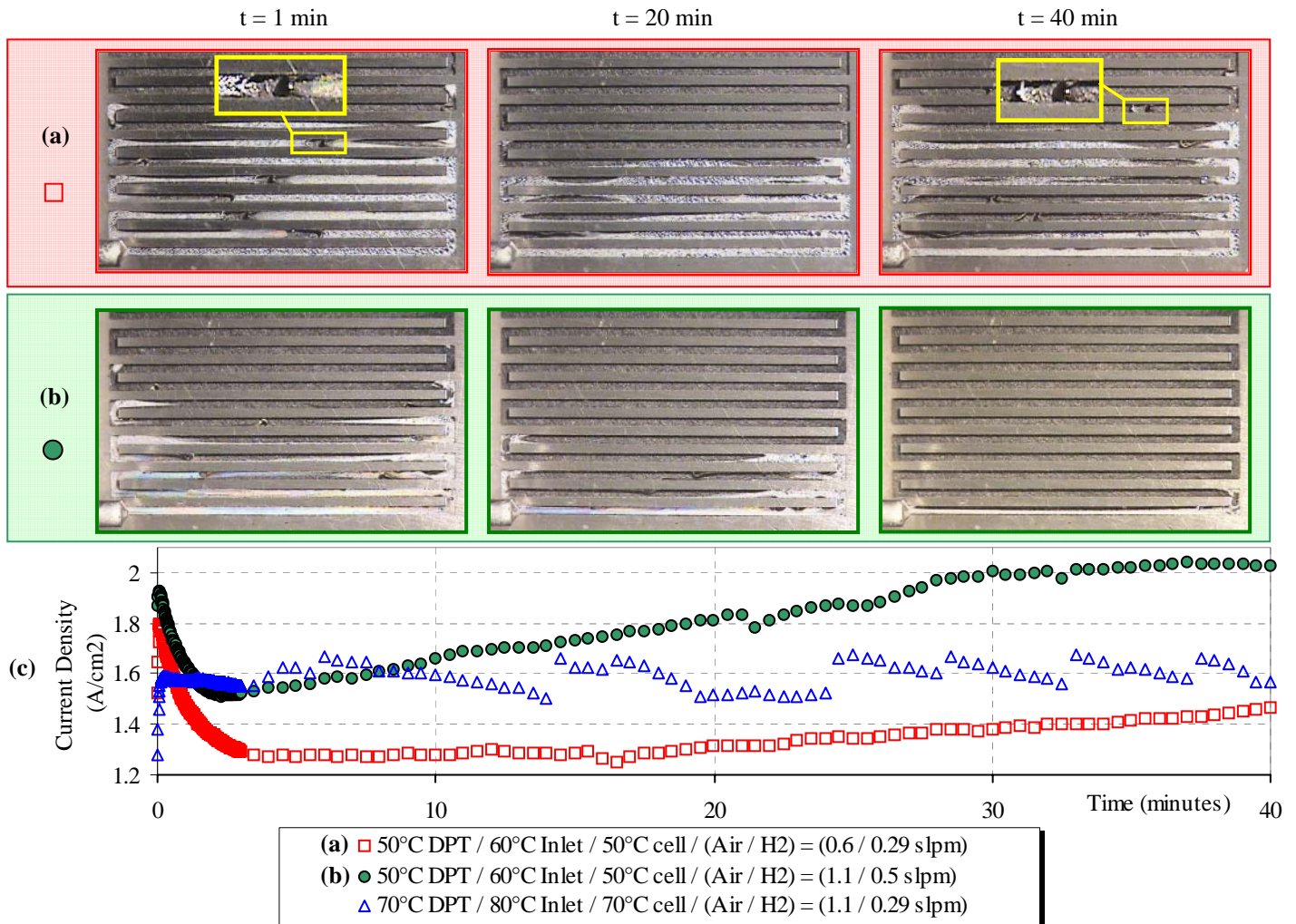


Fig. 5. Time evolution at constant voltage 0.4V after OCV, with SGL31BA as the GDL at different operating conditions: Cell performance (c) with the corresponding cathode flow field images (a) and (b)

liquid water was observed in the flow field, suggesting that the cell was operating at the membrane dehydration limit (also observed through fluctuations in the current output). Further increase of the air flow rate to 1.1 slpm (at 70°C) resulted in lower performance and higher current oscillations.

Influence of the GDL Material

Water management characteristics of different GDL materials were tested at the same operating conditions (Fig. 6). MEAs with MPL had SGL31BA on the anode side, while the MPL was facing the cathode catalyst layer. The level of the

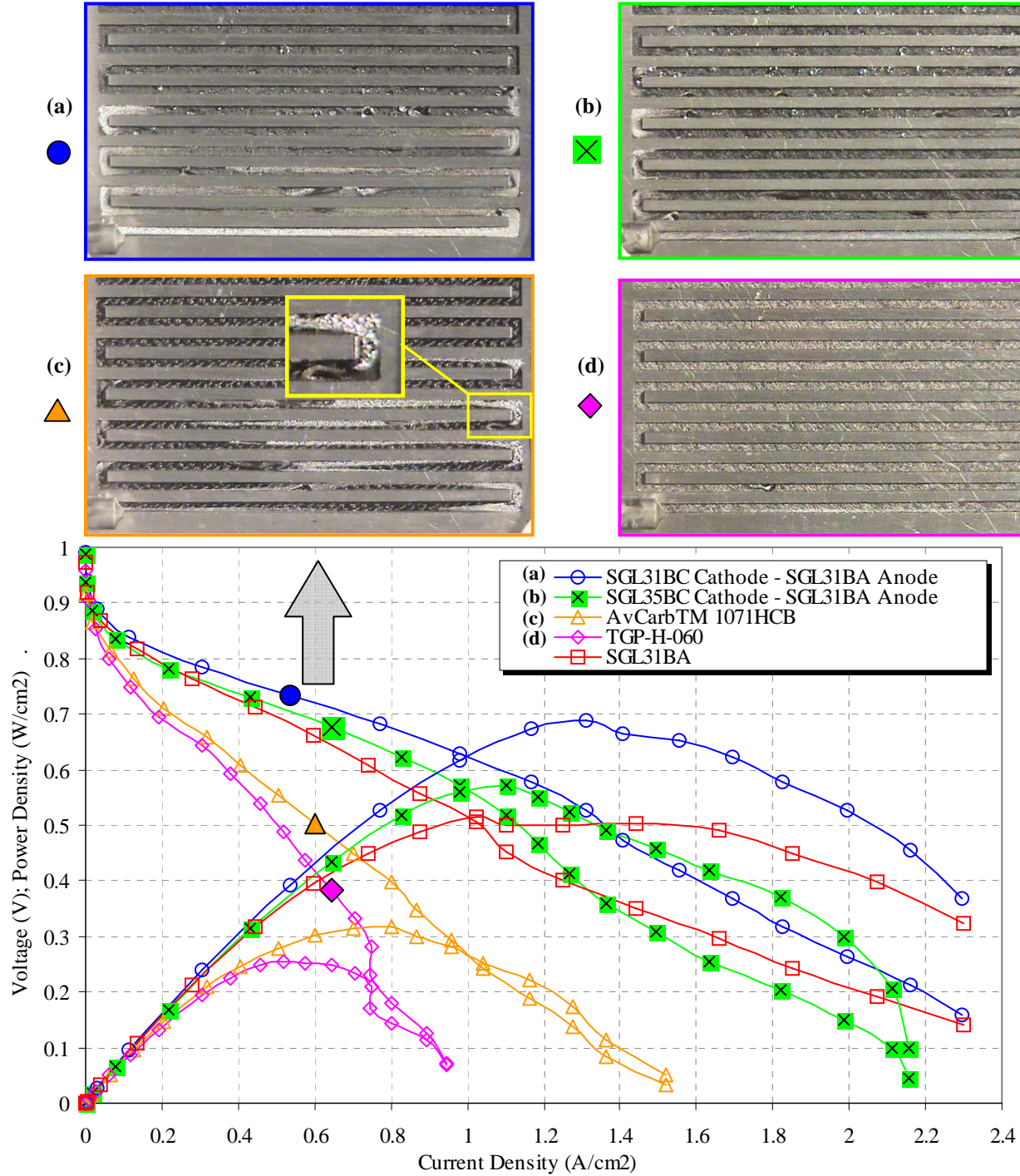


Fig. 6. Comparison of GDL materials at same operating conditions:
 50°C DPT/ 60°C Inlet / 50°C Cell / (Air / H₂) = (0.6 / 0.29 slpm)
 (a) – (d) Cathode flow field flooding compared at a similar current density

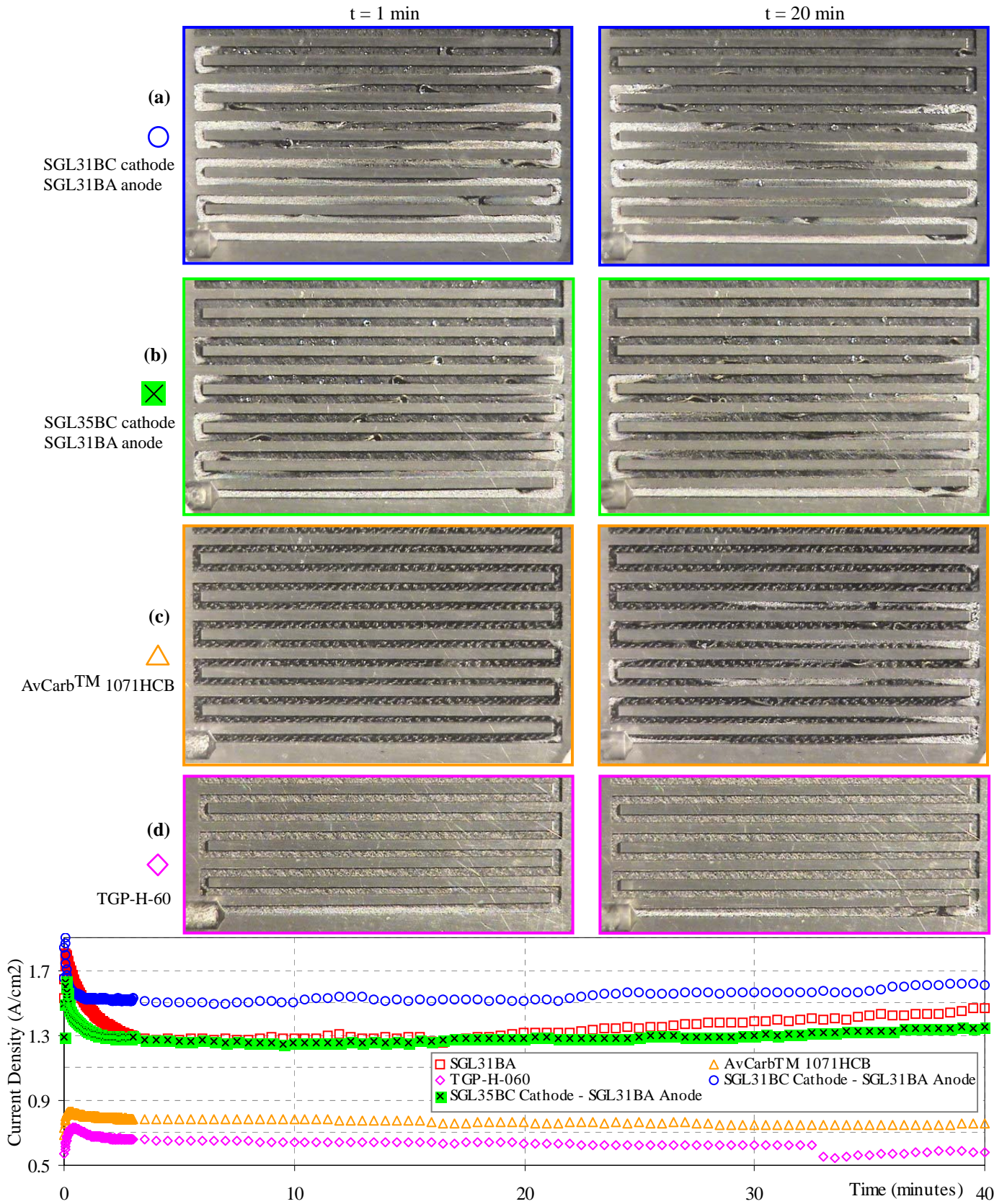


Fig. 7. Performance at constant voltage 0.4 V after OCV (same operating conditions as in Fig. 6)

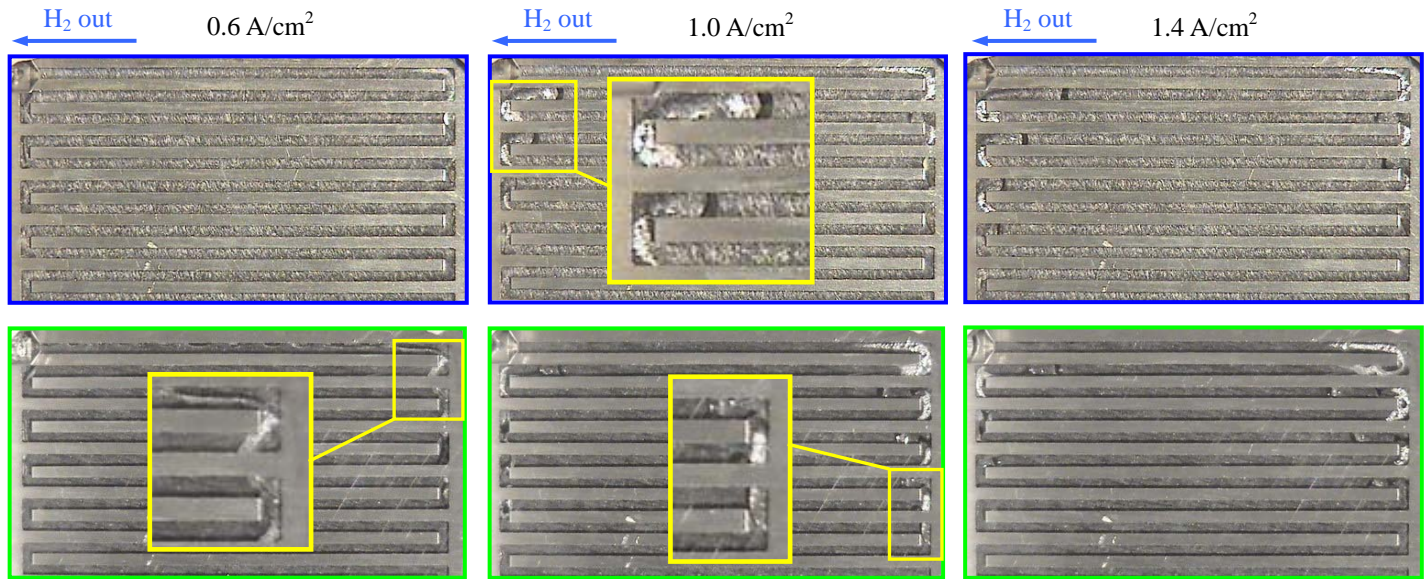


Fig. 8. Effect of MPL: Anode flow field flooding (same operating conditions as in Fig.6)
Top row: SGL31BC cathode / SGL31BA anode;
Bottom row: SGL35BC cathode / SGL31BA anode.

cathode flow field flooding was compared at similar current densities (i.e. similar water production rates). Images (a)–(d), Fig.6, correspond to the enlarged symbols on the polarization curves. (SGL31BA has been discussed earlier.) Although the water production rate is about the same, there is hardly any visible liquid water when GDL is Toray paper (Fig. 6d). We conclude that the water has been trapped inside the GDL and the catalyst layer, hence the poor performance (besides Toray's higher electrical resistance). We emphasize that one of the key roles of the GDL media is to prevent water condensation in the catalyst layer. Liquid water inside the flow field channels (when compared at same conditions and water production rate) means that excess water has been efficiently transported by the GDL away from the cathode.

Figure 7 illustrates the ability of GDL media to reach steady state for mass transport after step changes in cell current draw. Again, only traces of liquid water were observed close to the cathode outlet for Toray (although at lower current density). Furthermore, this material is very sensitive to occasional bursts of liquid water from the testing installation (small drop in current at about 35 minutes after switching from OCV to 0.4 V). SGL papers continue to operate under flooded cathode flow field. Although having an MPL does not necessarily result in better performance, it has an interesting influence on water dynamics, as discussed in the following section. As for the three GDLs without an MPL, we anticipated that higher cell performance was correlated with the higher in-plane permeability. SGL31BA had the highest in-plane permeability, and TGP-H-60 the lowest [12].

Effect of the Microporous Layer

Finally, we examined the influence of the microporous layer (structure shown in Fig. 2), by repeating the tests except that this time the anode side was visualized. No liquid water was observed in the anode flow field unless cathode GDLs had an MPL. MPL on the cathode side creates a pressure barrier for water produced at the catalyst layer. Water is pushed across the membrane to the anode side, resulting in anode flow field flooding and partial channel clogging close to the H₂ exit (Figs. 8, 9). Liquid water in the anode flow field indicates that the membrane is well hydrated, which is one of the major benefits provided by the MPL (through increased membrane ionic conductivity). In addition, MPL provides more intimate contact with the catalyst layer, thus decreasing the electrical contact resistance. Adding an MPL can also reduce the difference in performance between different GDLs [13].

Liquid water buildup at the anode side (Fig. 8) was observed while recording the polarization curves (very similar to curves in Fig. 6). Unlike the cathode side, where droplets emerge from the GDL pores, water on the anode side builds up from the channel walls as the unconsumed hydrogen reaches saturation before leaving the cell. Water accumulates at U-turns, probably promoted by imperfect temperature control. After exceeding a current density of about 1.7 A/cm², water is evaporated yielding a dry anode flow field. This could be explained as follows. At higher current density, the effect of electro-osmotic drag is more pronounced, decreasing the net water transport to the anode side. Second (and probably more influential), the experimental cell was cooled by natural convection only, resulting in a slightly increased cell temperature at high current densities (about 55-57°C at the limiting current, for cell heaters set at 50°C).

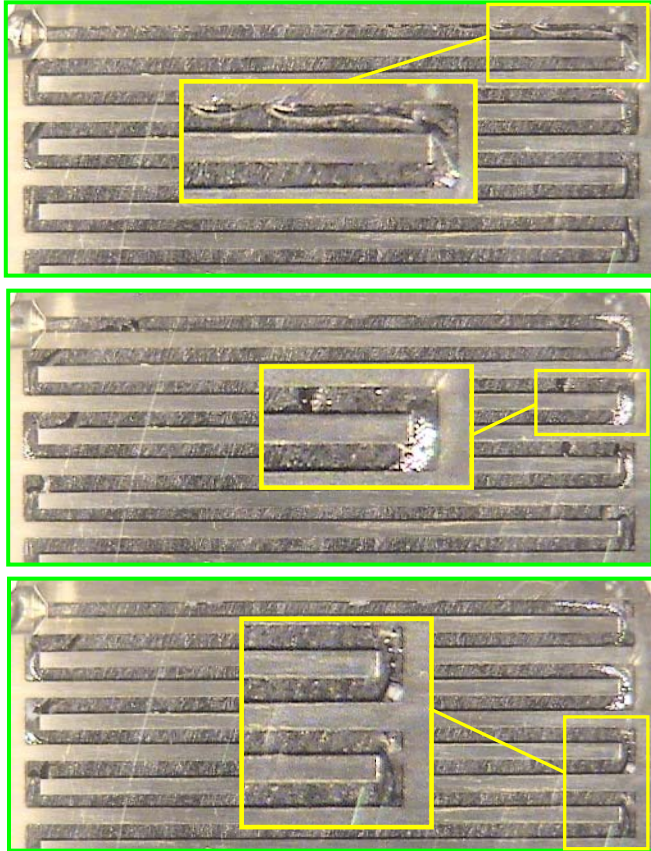


Fig. 9. Time evolution of the anode flow field flooding for SGL35BC cathode / SGL31BA anode at const 1.5 A/cm^2 after switching from OCV. *Top to bottom:* 5 min (0.5V); 10 min (0.51V); 120 min (0.42V).

The anode side was then visualized at constant currents (0.5 , 1 , and 1.5 A/cm^2) for 2 hours, after switching from OCV (Fig. 9). There was no visible water at OCV and 0.5 A/cm^2 . Slightly more water was observed at 1 A/cm^2 than at 1.5 A/cm^2 . The MPL effect was visible after just 1 minute, as water started to condense on the channel sidewall close to the outlet. Unlike the dynamic droplet movements observed on the cathode side, water is removed from the flow field mainly in vapor form.

Water condensation on the anode side was previously observed by neutron imaging [10]. Condensation occurred purely because of already saturated hydrogen feed (at very low flow rate), which was confirmed at open circuit conditions. In addition, GDLs employed in [10] did not have an MPL. However, no liquid water was observed in our experiments at open circuit (not even after running the cell at 0.5 A/cm^2 for two hours), whereas anode flow field flooding was obvious at higher current densities. We therefore conclude that water accumulation on the anode side was caused by water transport across the membrane, in addition to the water already carried into the cell by the humidified hydrogen feed. Clearly, this mechanism is competing with the electro-osmotic drag. To more carefully examine the influence of GDL/MPL materials

on the net water transport across the membrane, water collection apparatus for both sides of the cell will be added in our future experiments.

There are several effects that the MPL has on the water dynamics. First, saturated vapor pressure is higher inside the MPL, because of the smaller pore size (Fig. 2) and increased hydrophobicity. Therefore, the MPL is less prone to flooding. This effect is commonly modeled by the Kelvin equation [3, 4], although the validity of the equation might be questionable if the pores are too small. Second, it takes much higher pressure for the liquid water to break through the MPL pores. There is a subtle difference between the two effects, although both stem from the fact that the MPL pores are small and hydrophobic. A simple experiment (Fig. 10) illustrates the second effect: the water head was gradually increased in the acrylic tubes (2.5 cm diameter) with their bottom ends covered by GDL samples until water started to flow through the pores. Samples with an MPL had several times higher threshold water head. In order to achieve better performance through water management by the MPL, we conclude that the MPL properties need to be tailored for specific CCM, cell design, and operating conditions. For example, membrane material needs to be able to efficiently transport the water to the anode side. Further, if the MPL pressure barrier is too high, it might result in lower performance due to cathode catalyst flooding.

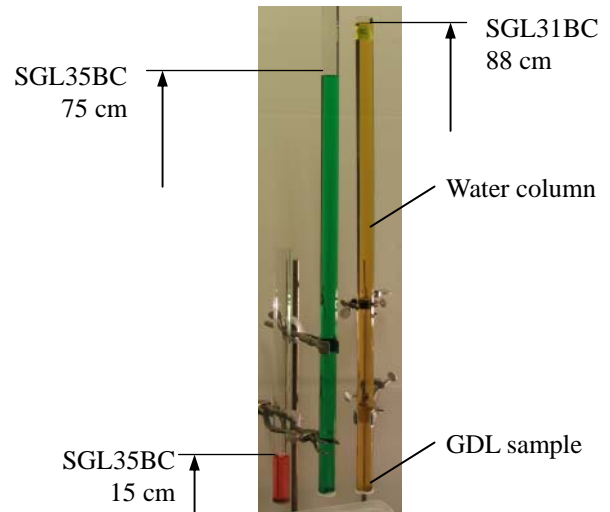


Fig.10. Threshold water head for the GDL samples

Two-Phase Flow: Single Serpentine vs. Parallel Flow Field

For the same air flow rate, Reynolds number is higher in the serpentine configuration, since the flow rate per cross section of a single channel is higher when compared to that of multiple parallel channels. Higher gas velocity and multiple U-turns make the two-phase transport more dynamic than in the parallel flow field. Further, when a parallel channel is blocked by liquid water, the air chooses a path of lesser resistance (through the remaining unblocked channels), thus leaving the

blocked channel starved of the reactant gas [6, 8]. The cell can continue to operate at significantly lower power output for extended periods due to the idle channel(s). On the other hand, only instantaneous serpentine channel blockage could be observed: air immediately either breaks through the blockage, or expels the accumulated water in the form of fast-moving slugs. In addition to evaporation and shear flow, another mechanism of water removal from the flow field is by collection of smaller stationary droplets by moving drops and slugs. Large drops and fast-moving slugs coalesce with, and sweep away, stationary droplets attached to the GDL or the wall surface thereby enhancing water removal. This is a dynamic process, and the active cell area changes in response to water movement along the channel, causing temporal fluctuations in cell power, rather than a sharp extended drop encountered in the parallel configuration. Further, water removal from the GDL is helped by the convective portion of the air flow under the lands, due to pressure difference between adjacent serpentine channel sections [14]. Liquid water accumulation at U-turns is characteristic for the serpentine flow field, as previously observed by neutron imaging [10]. Finally, it would be worthwhile to visualize the parallel anode flow field and check the influence of MPL on water management. We anticipate that prolonged anode channel blockage will occur under certain operating conditions, similar to that observed on the cathode side in previous parallel flow field studies [6, 8].

Conclusions

Two-phase dynamics were investigated by experimental visualization for different GDL materials for the first time in a single-serpentine hydrogen-air PEMFC. This experimental approach has shown to be very useful to examine the influence of water management characteristics of GDL materials on the cell performance and liquid water transport. GDL on the cathode side plays a key role in removing the excess water away from the catalyst layer and through the flow field channel. Inside the channel, liquid water can move in the form of droplets, films and fast-moving slugs. Surface properties of the GDL and channel walls are vital for the efficient liquid water removal, and are subject of our ongoing research. Well designed GDL media characterization is needed to improve the cell performance by material design.

Water condensation in the anode flow field was observed visually for the first time. Water was pushed across the membrane to the anode side as the effect of the pressure barrier introduced when MPL was used on the cathode side. Tailoring the MPL will improve the water management and consequently the efficiency of the fuel cell.

Acknowledgements

We acknowledge funding for this research by the US Department of Energy grant DE-FG02-04ER63820, and Delaware Natural Resource and Environmental Control (DENREC) award No. 01040000450. The authors would also

like to thank Mr. Dan McCluskey of SGL Carbon Group for providing the GDL samples with MPL.

References

- [1] Larminie, J., and Dicks, A., 2001, *Fuel Cell Systems Explained*, John Wiley & Sons LTD, Chap.4.
- [2] He, W., Lin, G. and Nguyen, T. V., 2003, "Diagnostic Tool to Detect Electrode Flooding in Proton-Exchange-Membrane Fuel Cells", *AIChE J.* **49** (12), pp. 3221-3228.
- [3] Weber, A.Z., Darling, R.M., and Newman, J., 2004, "Modeling Two-Phase Behavior in PEFCs", *J. Electrochem. Soc.*, **151** (10), pp. 1715-1727.
- [4] Weber, A.Z., Darling, R.M., and Newman, J., 2005, "Effects of Microporous Layers in Polymer Electrolyte Fuel Cells", *J. Electrochem. Soc.*, **152** (4), pp. 677-688.
- [5] Hakenjos, A., Muentert, H., Wittstadt, U., and Hebling, C., 2004, "A PEM Fuel Cell for Combined Measurement of Current and Temperature Distribution, and Flow Field Flooding", *J. Power Sources*, **131**, pp. 213-216.
- [6] Tüber, K., Pócza, D., and Hebling, C., 2003, "Visualization of Water Buildup in the Cathode of a Transparent PEM Fuel Cell" *J. Power Sources*, **124**, pp. 403-414.
- [7] Barbir, F., Gorgun, H., and Wang, X., 2005, "Relationship between Pressure Drop and Cell Resistance as a Diagnostic Tool for PEM Fuel Cells", *J. Power Sources*, **141**, pp. 96-101.
- [8] Yang, X. G., Zhang, F. Y., Lubawy, A. L., and Wang, C. Y., 2004, "Visualization of Liquid Water Transport in a PEFC", *Electrochem. Solid-State Lett.*, **7** (11), pp. 408-411.
- [9] Sugiura, K., Nakata, M., Yodo, T., Nishiguchi, Y., Yamauchi, M., and Itoh, Y., 2005, "Evaluation of a Cathode Gas Channel with a Water Absorption Layer/Waste Channel in a PEFC by Using Visualization Technique", *J. Power Sources*, **145**, pp. 526-533.
- [10] Pekula, N., Heller, K., Chuang, P.A., Turhan, A., Mench, M.M., Brenizer, J.S., and Ünlü, K., 2005, "Study of Water Distribution and Transport in a Polymer Electrolyte Fuel Cell Using Neutron Imaging", *Nucl. Instrum. Methods Phys. Res., Sect. A*, **542**, pp. 134-141.
- [11] Tsushima, S., Teranishi, K., and Hirai, S., 2004, "Magnetic Resonance Imaging of the Water Distribution within a Polymer Electrolyte Membrane in Fuel Cells", *Electrochem. Solid-State Lett.*, **7** (9), pp. 269-272.
- [12] Feser, J.P., 2005, "Convective flow through polymer electrolyte fuel cells", M.S. thesis, University of Delaware
- [13] Qi, Z., and Kaufman, A., 2002, "Improvement of Water Management by a Microporous Sublayer for PEM Fuel Cells", *J. Power Sources*, **109**, pp. 38-46.
- [14] Williams, M.V., Kunz, H.R., and Fenton, J.M., 2004, "Influence of Convection Through Gas-Diffusion Layers on Limiting Current in PEM FCs Using a Serpentine Flow Field", *J. Electrochem. Soc.*, **151** (10), pp. 1617-1627.